Title

The Tyrosine Kinase Inhibitor Gefitinib Restricts Mycobacterium tuberculosis Growth through Increased Lysosomal Biogenesis and Modulation of Cytokine Signaling

Journal

ACS Infectious Diseases, 3(8)

ISSN

2373-8227

Authors

Sogi, Kimberly M
Lien, Katie A
Johnson, Jeffrey R
et al.

Publication Date

2017-08-11

DOI

10.1021/acsinfecdis.7b00046

Peer reviewed

HHS Public Access

Author manuscript

ACS Infect Dis. Author manuscript; available in PMC 2018 August 11.

Published in final edited form as:

ACS Infect Dis. 2017 August 11; 3(8): 564–574. doi:10.1021/acsinfecdis.7b00046.

The Tyrosine Kinase Inhibitor Gefitinib Restricts *Mycobacterium tuberculosis* Growth through Increased Lysosomal Biogenesis and Modulation of Cytokine Signaling

Kimberly M. Sogi[†], **Katie A. Lien**[‡], **Jeffrey R. Johnson**[#], **Nevan J. Krogan**[#], and **Sarah A. Stanley**[†,‡,*]

[†]School of Public Health, Division of Infectious Diseases and Vaccinology, Li Ka Shing Center, University of California, Berkeley, California 94720, United States

[‡]Department of Molecular and Cell Biology, University of California, Berkeley, California 94720, United States

[#]Department of Cellular and Molecular Pharmacology, University of California—San Francisco, San Francisco, California 94158, United States

Abstract

Host-directed therapeutics have the potential to combat the global tuberculosis pandemic. We previously identified gefitinib, an inhibitor of EGFR, as a potential host-targeted therapeutic effective against *Mycobacterium tuberculosis* infection of macrophages and mice. Here we examine the functional consequences of gefitinib treatment on *M. tuberculosis* infected macrophages. Using phosphoproteo-mic and transcriptional profiling, we identify two mechanisms by which gefitinib influences macrophage responses to infection to affect cytokine responses and limit replication of *M. tuberculosis* in macrophages. First, we find that gefitinib treatment of *M. tuberculosis* infected macrophages inhibits STAT3, a transcription factor known to repress effective immune responses to *M. tuberculosis* in vivo. Second, we find that gefitinib treatment of *M. tuberculosis* infected macrophages leads to increased expression of genes involved in lysosomal biogenesis and function and an increase of functional lysosomes in gefitinib treated cells. Furthermore, we show that gefitinib treatment increases the targeting of bacteria to

[*]Corresponding Author: (S.A.S.) sastanley@berkeley.edu.

ORCID

Kimberly M. Sogi: 0000-0002-4011-2440

Sarah A. Stanley: 0000-0002-4182-9048

Notes

The authors declare no competing financial interest.

Supporting Information

The Supporting Information is available free of charge on the ACS Publications website at DOI: 10.1021/acsinfec-dis.7b00046. Figure S1: Western blot of pSTAT3, STAT3, and actin from cell lysates of $STAT3^{+}$ and $STAT3^{-}$ macrophages infected with *M. tuberculosis* at 24 h post-infection. Figure S2: Fluorescent images of BMDM infected with *M. tuberculosis* expressing GFP, fixed at 24 h post-infection, and stained with a LAMP1-AF647 antibody. Quantification of LAMP1 staining by Cell Profiler. Figure S3: Proposed model for gefitinib activity on *M. tuberculosis* infected macrophages. Table S1: Summary of phosphosites significantly changed in *M. tuberculosis* infected macrophages versus mock infected macrophages and *M. tuberculosis* infected macrophages with and without gefitinib. Table S2: Summary of all phosphosites significantly changed in *M. tuberculosis* infected macrophages versus mock infected macrophages. Table S3: Summary of phosphosites significantly changed in *M. tuberculosis* infected macrophages with and without gefitinib. Table S4: RNaseq data listing all genes that were >2 times up- or down-regulated in response to gefitinib in *M. tuberculosis* infected macrophages (PDF)

lysosomes, providing an explanation for the cell intrinsic effects of gefitinib treatment on *M. tuberculosis* infection. Our data provide novel insights into the effects of gefitinib on mammalian cells and into the possible roles for EGFR signaling in macrophages.

Graphical abstract

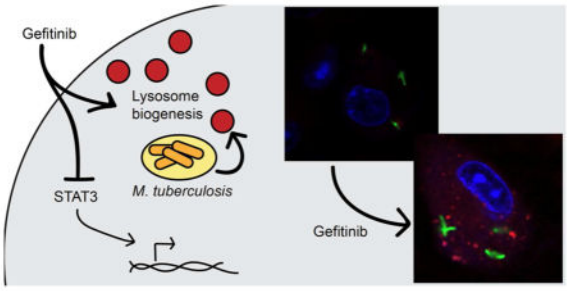

Keywords

Mycobacterium tuberculosis; host-directed therapeutic; lysosomal biogenesis; signal transducer and activator of transcription 3 (STAT3); epidermal growth factor receptor (EGFR)

Mycobacterium tuberculosis is a global pathogen that infects one-third of the world population. In 2015 the WHO estimated that there were 10 million new cases and almost half a million new multidrug-resistant cases worldwide.[1] Despite increasing oversight in the administration of antituberculosis drugs, several conditions have promoted the rise in drug-resistant strains. These conditions include the prolonged chemotherapy regimens necessary to treat tuberculosis, drug side effects that lead to poor adherence, poor penetration into lesions of specific drugs, and pharmocokinetic/pharmacodynamic mismatches in front-line drugs.[2] The rapid rise of drug resistance even to new drugs and novel therapeutic targets continues to be an urgent concern.[3] Recent years have seen an increase in research toward identifying host-directed therapies (HDT) that could be used in conjunction with current antimycobacterial chemotherapies to shorten treatment times, with the added benefit of being less susceptible to the development of drug resistance. To date, a wide variety of HDT have been identified with a few currently in clinical trials.[4] Importantly, many of the HDT with activity against tuberculosis were first identified and used as therapeutics for other clinical contexts and thus are known to be safe and efficacious against their targets in humans. Research on HDT for tuberculosis has revealed a wide range of potential targets. The mechanism of HDT can be broadly categorized into three types: blocking host pathways that are beneficial to *M. tuberculosis* growth, increasing protective immune mechanisms that enhance pathogen elimination, and limiting damaging inflam-matory responses.[5] HDT not only represent novel therapeutic strategies but also provide new tools to study the *M. tuberculosis* host–pathogen interaction.

Previously we screened a library of host-targeted inhibitors in a macrophage infection model of *M. tuberculosis* to identify novel host-targeted therapeutics and discover new pathways that could lead to control of *M. tuberculosis* infection.[6] This screen identified both previously identified targets from other studies as well as novel targets. We identified eight

inhibitors of the epidermal growth factor receptor (EGFR) tyrosine kinase family that block replication of *M. tuberculosis* in macrophages, including gefitinib, an FDA-approved EGFR inhibitor. Importantly, we found that mice infected with *M. tuberculosis* had fewer bacteria in their lungs after only four doses of gefitinib treatment, demonstrating the relevance of this pathway in vivo.[6] The EGFR family of receptors (Erb receptors) plays an important role in cellular development, proliferation, differentiation, survival, and migration.[7] The Erb family contains four tyrosine receptor kinases, each binding to a different profile of activating ligands, with the exception of ErbB2, which lacks a ligand-binding domain and functions to enhance signaling through Erb receptors via heterodimeriza-tion.[8] Aberrant or excessive signaling through EGFR and/or ErbB2 can contribute to solid tumor development. Due to its role in cancer development and progression, many inhibitors of EGFR and ErbB2 have been developed.[7] Gefitinib is currently used to treat a subset of non-small-cell lung cancer that expresses a mutated form of EGFR and is known to be tolerated in chronic administration,[9] a necessary condition for potential use as an adjunct therapy for treatment of tuberculosis in humans.

Several studies implicate EGFR signaling in the pathogenesis and control of infectious diseases. EGFR has been linked to influenza uptake, regulation of inflammation following rhinovirus infection, and prevention of apoptosis in bacterially infected gastric epithelial cells.[10–12] EGFR signaling has not previously been implicated in control of *M. tuberculosis* infection and was not identified in any of the previous genome-wide screens.[13–15] However, two studies have shown a direct role of EGFR signaling in promoting the pathogenesis of intracellular pathogens. *Mycobacterium leprae* directly activates ErbB2 signaling in Schwann cells, resulting in myelin damage and disease pathogenesis,[16] and *Toxoplasma gondii* activates EGFR signaling to suppress autophagy and promote parasite survival in endothelial and epithelial cells.[17] In addition, EGFR signaling has been shown to modulate the activation of macrophages in tumor environments and in models of experimental colitis.[18,19] In sum, these studies suggest a role for EGFR signaling that can be utilized by both pathogens and the host for modulating macrophage activation and functions during infection.

The role of EGFR/ErbB2 signaling during *M. tuberculosis* infection is not known. We used a small molecule inhibitor of EGFR and ErbB2, gefitinib, to investigate how inhibition of EGFR/ErbB2 signaling restricts *M. tuberculosis* growth in macrophages. We used phosphoproteomics and whole tran-scriptome sequencing (RNA-seq) to identify novel pathways affected by gefitinib treatment of *M. tuberculosis* infected macrophages in an unbiased manner. The phosphoproteomic profiling indicated that gefitinib treatment significantly changed the levels of phosphorylation on signal transducer and activator of transcription 3 (STAT3), a transcription factor that has been shown to impair effective immune responses to *M. tuberculosis*.[20] Using macrophages lacking STAT3, we showed that gefitinib restriction of *M. tuberculosis* growth is independent of STAT3 at the cellular level; however, it may promote the activity of gefitinib in vivo. Transcriptional profiling indicated that a number of lysosomal genes were induced by gefitinib treatment of *M. tuberculosis* infected macrophages. Using fluorescent microscopy, we found a dramatic increase in lysosomes in gefitinib-treated macrophages. We find that these lysosomes are functional and observed increased targeting of *M. tuberculosis* to lysosomes in gefitinib-treated cells. This

work identifies novel effects of gefitinib treatment on mammalian cells that may have relevance in numerous disease settings including cancer, inflammation, and infectious disease.

RESULTS AND DISCUSSION

Gefitinib Activity in *M. tuberculosis* Infected Macrophages Does Not Result from Enhanced NO Production or Increased Autophagy

Previously we showed that gefitinib treatment limits *M. tuberculosis* growth in resting macrophages.[6] The cytokine interferon-γ (IFN-γ) plays an essential role in the activation of macrophages to control *M. tuberculosis* infection. IFN-γ activation has been proposed to result in bacterial control via increased expression of the inducible nitric oxide synthase (iNOS), which produces the toxic radical nitric oxide (NO), and via enhanced flux through autophagy.[21,22] As a first step in identifying the mechanism of action, we tested whether gefitinib treatment synergizes with IFN-γ activation to control *M. tuberculosis* in mouse bone marrow derived macrophages (BMDM). To assess growth, we used a luminescent reporter strain, TB-Lux, that expresses the bacterial luminescent operon *lux*CDABE that we have shown to be a linear reporter of bacterial number in macrophages.[23] Resting and IFN-γ-activated BMDM were infected with TB-lux and treated with gefitinib or gefitinib and IFN-γ for 4 days post-infection. As expected, gefitinib treatment inhibited replication of *M. tuberculosis* in macrophages, as did activation of the macrophages with IFN-γ (Figure 1A). However, the combination of gefitinib treatment and IFN-γ activation resulted in only a small additional effect on *M. tuberculosis* control (Figure 1A), suggesting that gefitinib may activate a pathway in macrophages that is already activated by IFN-γ. We therefore tested whether gefitinib activates pathways known to be essential for IFN-γ mediated control. To test whether gefitinib induces NO production, we infected BMDM with *M. tuberculosis* and treated with gefitinib. At 24 h post-infection, we measured the levels of nitrite, a byproduct of NO production, in the supernatants. As expected, BMDM pretreated with IFN-γ prior to *M. tuberculosis* infection produced high levels of NO. However, gefitinib treatment did not enhance NO production in macrophages compared to untreated controls, demonstrating that gefitinib does not restrict *M. tuberculosis* growth in macrophages by increasing NO production (Figure 1B). In addition, there was no change in the transcript levels of iNOS (not shown).

Autophagy, a process that allows infected cells to target intracellular pathogens to lysosomes for degradation, has been a popular target for HDT of tuberculosis.[5] To assess induction of autophagy by gefitinib, we measured the conversion of the autophagy effector microtubule-associated protein 1A/1B-light chain 3 (LC3) from its inactive state (LC3-I) to its lipidated active state (LC3-II) by Western blot.[24] As expected, we found that treatment with chloroquine (CQ), an inhibitor that interferes with lysosomal hydrolysis through multiple mechanisms, resulted in enhanced accumulation of LC3-II (Figure 1C). *M. tuberculosis* infected macrophages treated with gefitinib showed more LC3 conversion than untreated cells (Figure 1C). These data indicate that gefitinib treatment induces flux through autophagy, suggesting that autophagy might account for the activity of gefitinib against *M. tuberculosis* in macrophages. To test if gefitinib increases the targeting of *M. tuberculosis* to

autophagosomes, we measured the co-localization of LC3 and fluorescent *M. tuberculosis* in BMDM expressing LC3-GFP. We found that there was no difference in LC3 co-localization with bacteria in gefitinib-treated cells compared to untreated (Figure 1D), suggesting that the enhanced flux through autophagy indicated by LC3 conversion does not result in specific targeting of *M. tuberculosis* to the autophagic pathway. To rule out a role for autophagy, we tested whether gefitinib is capable of restricting *M. tuberculosis* growth in macrophages that lack the core autophagy effector Atg7 and are unable to induce autophagy.[24] We assessed the growth of *M. tuberculosis* in BMDM derived from Atg7 flox/flox LysMcre −/− ($Atg7^{+}$) and Atg7 flox/flox LysMcre +/+ ($Atg7^{-}$) mice. We confirmed that $Atg7^{-}$ macrophages were defective for LC3 conversion by Western blot (Figure 1E). Gefitinib treatment was effective at restricting *M. tuberculosis* growth in both $Atg7^{+}$ and $Atg7^{-}$ macrophages (Figure 1F), suggesting the increased flux through autophagy indicated by enhanced LC3 conversion does not explain gefitinib's activity. Although the amount of LC3-II can correlate with the number of autophagosomes, LC3-II can also accumulate as a result of defective autophagy or lysosomal function.[25] Although gefitinib treatment of macrophages clearly enhances LC3 conversion, the results above clearly demonstrate that autophagy is not the mechanism by which gefitinib limits *M. tuberculosis* replication in macrophages.

Phosphotyrosine Analysis Shows an Inverse Regulation of Signaling with Gefitinib Treatment Compared to Untreated *M. tuberculosis* Infected Macrophages

To identify signaling pathways inhibited by gefitinib, we used global phosphoproteomics to comprehensively profile tyrosine kinase signaling in *M. tuberculosis* infected macrophages with and without gefitinib treatment. Macrophages were infected with *M. tuberculosis* using a 4 h phagocytosis period, after which time gefitinib treatment was initiated ($t = 0$) (Figure 2A). Protein extracts were prepared from uninfected, infected treated with DMSO, and infected treated with gefitinib macrophages at 4 and 8 h. Proteins were digested with trypsin and phosphopeptides enriched using iron(III) immobilized metal ion affinity chromatography. Peptides containing phosphotyrosine residues were further enriched using an anti-phosphotyrosine antibody and analyzed by label-free mass spectrometry. We detected a total of 994 phosphotyrosine sites across all time points and conditions. Approximately 60 phosphosites exhibited altered abundance in response to *M. tuberculosis* infection across the 4 and 8 h time points (Figure 2B). Comparison of changes in phosphotyrosine signaling resulting from *M. tuberculosis* infection with a curated database of published phosphoproteomics using PhosFate[26] strongly correlated with other phosphoproteomic studies of cells infected with the bacterial pathogens *Shigella flexneri*[27] and *Salmonella enterica*[28] in epithelial cells (Figure 2C). Interestingly, *M. tuberculosis* infection of macrophages also correlated with EGF treatment of epithelial cells and has an inverse correlation with epithelial cells activated with EGF and treated with a MAPK inhibitor[29] (Figure 2C). This is suggestive that *M. tuberculosis* infection activates similar signaling pathways to the activation of EGFR by EGF treatment. Comparison of gefitinib treated to untreated infected macrophages resulted in changes in abundance of 57 phosphopeptides across the two time points, with 32 sites being down-regulated (Figure 2B). Importantly, we observed that several known EGFR targets exhibited decreased phosphorylation upon treatment with gefitinib, including Src family kinases (Lyn and Hck) and phospholipase C family proteins (PLCγ) (Table S2). Hierarchical clustering of the data

using phosphopeptides identified in every condition, and significant in at least one comparison, revealed two primary clusters characterized by changes in protein cellular catabolism (cluster 1) or regulation of the innate immune response (cluster 2) (Figure 2D). Generally, gefitinib treatment reverses changes observed as a result of *M. tuberculosis* infection, demonstrating that gefitinib has a major impact on phosphotyrosine signaling in *M. tuberculosis* infected macrophages and that gefitinib's effect as a host-directed therapy enhances cell intrinsic control of *M. tuberculosis* infection.

Phosphoproteomic Analysis and Transcriptional Profiling Reveal STAT3 Signaling as a Major Pathway Affected by Gefitinib Treatment of *M. tuberculosis* Infected Macrophages

Pathway analysis of the phospho-proteomic data revealed a network of interacting proteins with gefitinib-induced changes in phosphorylation that included signal transducer and activator of transcription-3 (STAT3), a known regulator of *M. tuberculosis* infection (Figure 3A). Infection of macrophages with *M. tuberculosis* resulted in a significant increase in STAT3 phosphorylation of tyrosine 705 at 4 h after infection that was inhibited by treatment with gefitinib (Table S1). These data suggest that STAT3-dependent transcriptional activation is inhibited by treatment with gefitinib. In parallel experiments, we performed transcriptional profiling to identify pathways activated or inhibited by gefitinib treatment during *M. tuberculosis* infection at 4 and 24 h post-infection. Macrophages were infected with *M. tuberculosis* and treated with gefitinib after the 4 h phagocytosis period, and RNA was prepared at 4 and 24 h after gefitinib treatment. Using the cutoff of a 2-fold change in expression with a p value of <0.05, we found that *M. tuberculosis* infection alone affected the expression levels of 1415 and 584 transcripts at 4 and 24 h, respectively. Treatment of *M. tuberculosis* infected macrophages with gefitinib resulted in changes in expression levels of 965 and 973 transcripts at 4 and 24 h, respectively, compared to infection alone. Using ingenuity pathway analysis, signal transducer and activator of transcription 3 (STAT3) emerged as a major upstream regulator of genes differentially expressed upon gefitinib treatment at 4 h after infection (z score = −1.67, p value = 6.0×10^{-4}), corroborating our phosphoproteomic analysis (Figure 3B). Taken together, this global profiling suggests that inhibition of STAT3 signaling is a major outcome of gefitinib treatment of *M. tuberculosis* infected macrophages.

Gefitinib Inhibits STAT3-Dependent Macrophage Cytokine Responses

To determine if STAT3 phosphor-ylation is important for gefitinib activity, we first validated the STAT3 phosphoproteomic results by Western blot for STAT3 phosphorylation. Treatment with gefitinib significantly reduced STAT3 phosphorylation in *M. tuberculosis* infected cells, validating the phosphoproteomic data (Figure 3C). STAT3 is thought to impair host responses to *M. tuberculosis* infection by suppressing iNOS expression[30] and by modulating the expression of inflammatory cytokines[31,32] and therefore has effects on *M. tuberculosis* infection both at the level of the infected macrophages and in the production of cytokines that influence T cell responses in vivo. Activated STAT3 results in transcription of suppressor of cytokine signaling 3 (SOCS3), an inhibitor of STAT3 that has been shown to be important for host defense against *M. tuberculosis*. Mice lacking SOCS3 in macrophages are unable to restrain STAT3 signaling and are susceptible to *M. tuberculosis* infection.[33] To establish if STAT3 signaling is necessary for gefitinib-mediated *M. tuberculosis* restriction

in macrophages, we bred STAT3$^{flox/flox}$ mice to LysM-cre mice to generate mice with STAT3-defficient macrophages. We used macrophages derived from STAT3 flox/flox LysMcre +/− (STAT3^{-}) mice, which had very low levels of STAT3 expression as determined by Western blot (Figure S1). We infected STAT3^{-} macrophages with *M. tuberculosis* and measured bacterial growth by CFU with and without gefitinib treatment. Gefitinib was able to restrict growth of *M. tuberculosis* in both STAT3^{+} and STAT3^{-} macrophages to the same degree, suggesting that gefitinib-mediated restriction is not due to the inhibition of STAT3 signaling for cell intrinsic control (Figure 3D). This is consistent with the published finding that SOCS3, a negative regulator of STAT3, is dispensable for control of *M. tuberculosis* infection in macrophages in vitro, but is critical in vivo.[20] During in vivo infection, SOCS3 functions to prevent excessive IL-6/STAT3 signaling in macrophages that leads to decreased IL-12 production and impaired T cells responses.[33] It is known that IL-12 production is required for the optimal development of Th1 T cells that produce IFN-γ and provide the most important component of host immunity to *M. tuberculosis*.[34] Taken together, these findings raise the possibility that the in vivo activity of gefitinib might result in part from inhibition of STAT3 signaling, which would lead to decreased IL-6 production, increased IL-12 production, and improved T cell responses to infection. In support of this hypothesis, we found that *M. tuberculosis* infection induced robust production of IL-6 and that gefitinib treatment significantly inhibited IL-6 production (Figure 3E). We were unable to detect IL-12 mRNA in our RNA-seq data or protein by ELISA from supernatants 24 h post-infection with *M. tuberculosis* (data not shown). However, gefitinib may enhance IL-12 production by macrophages in vivo. Furthermore, STAT3 signaling in T cells is also detrimental to host defense against *M. tuberculosis* infection,[35] raising the possibility that gefitinib acts on cells other than macrophages in vivo. Finally, although STAT3 is a known target of EGFR signaling,[36] STAT3 signaling in macrophages is thought to be primarily regulated by cytokines.[35] Thus, it is surprising that gefitinib treatment results in a dramatic decrease in STAT3 activation, suggesting the interesting possibility that EGFR signaling modulates cytokine responses of macrophages during *M. tuberculosis* infection.

Gefitinib Treatment of Infected Macrophages Increases Lysosomal Number and Increases *M. tuberculosis* Trafficking to Lysosomes

Although inhibition of STAT3 signaling may contribute to gefitinib activity in vivo, we found that STAT3 plays no role in cell intrinsic control of infection. We therefore sought alternative explanations for gefitinib's antimicrobial effects in macrophages. From our RNA-seq data, we identified a number of genes related to lysosomal function that were up-regulated by gefitinib treatment (Figure 4A). Notably, we found that the expressions of several cathepsin genes (*ctsa*, *ctsb*, and *ctsd*) were enhanced upon gefitinib treatment. Cathepsins are proteases that are found in the lysosome and contribute to the degradative capacity of this organelle.[37] In addition, we observed increased expression of other lysosomal genes including LAMP1, NPC2, and subunits of the vacuolar ATPase. These data suggested that lysosomal function and/or biogenesis might be enhanced by gefitinib treatment, and we therefore examined lysosomes in gefitinib-treated macrophages using lysotracker, an acid-sensitive fluorescent dye that accumulates in acidic cellular compartments. Treatment of *M. tuberculosis* infected macrophages with gefitinib resulted in a striking increase in the number of lysotracker-positive vesicles at 24 h after infection

(Figure 4B,C). To validate that lysotracker staining was labeling lysosomes, we also performed immunofluorescence staining of the lysosomal marker LAMP1 and saw an increase in overall LAMP1 staining in gefitinib-treated macrophages compared to untreated controls (Figure S2). We next sought to determine whether the observed increase in lysosomes in gefitinib treated macrophages resulted in an increase of bacteria trafficking to lysosomes. Using a GFP-expressing *M. tuberculosis* strain, we measured the co-localization of fluorescent *M. tuberculosis* with lysotracker-labeled lysosomes in macrophages treated with gefitinib. Using Cell Profiler to analyze the images, we measured the number of bacteria in lysosomes compared to the total number of bacteria in infected macrophages at 24 h after infection. We found that gefitinib treatment of macrophages significantly increases the co-localization of *M. tuberculosis* to lysosomes (Figure 4D).

Gefitinib Induces Functional Lysosomes

Like many drugs with weakly basic moieties, it is possible that gefitinib is trapped in lysosomes.[38] This raises two possibilities: that gefitinib accumulates in lysosomes to concentrations at which it may have direct activity against bacteria and that gefitinib induces phospholipidosis and dysfunctional lysosomes. To address the first possibility, we tested gefitinib for direct *M. tuberculosis* growth inhibition in broth culture and on solid media and were unable to measure a change in growth up to 1 mM, the limit of gefitinib solubility (not shown). In addition, we were unable to generate resistant mutants to gefitinib by passaging *M. tuberculosis* through gefitinib-treated macrophages (48 bacterial doublings). Although we cannot rule out the possibility that gefitinib is directly inhibiting *M. tuberculosis* growth, our experiments suggest that it is unlikely and that gefitinib may indeed act primarily by enhancing host microbicidal mechanisms. We next addressed the possibility that lysosomal accumulation of gefitinib could interfere with lysosomal function. Previous studies have shown that lysomotropic molecules can disrupt the acidification of lysosomes and therefore inhibit lysosomal enzymes and degradative capacity.[38] However, gefitinib treatment results in enhanced lysotracker staining, whereas lysomotropic agents quench lysotracker fluorescence.[38] We found that gefitinib treatment of macrophages increases expression of cathepsins, which require proteolytic activation and an acidic environment before they are fully active. We tested the proteolytic capacity of gefitinib-induced lysosomes by treating cells with bovine serum albumin (BSA) conjugated to BODIPY (DQ-BSA), which is taken up through micropinocytosis and fluoresces after proteolysis in lysosomes. We found that in both untreated and gefitinib-treated macrophages the majority of lysotracker-positive compartments were also positive for DQ-BSA proteolysis (Figure 5A). In addition, we observed an increase in overall staining with DQ-BSA after gefitinib treatment similar to what we observed with lysotracker and LAMP-1 staining (Figure 5B). Thus, gefitinib treatment leads to a significant increase in the number of functional lysosomes in the macrophages.

M. tuberculosis Mutants That Exhibit Increased Trafficking to Lysosomes Are More Susceptible to Killing in Gefitinib-Treated Macrophages

Localization to lysosomes is thought to be an important mechanism by which macrophages control *M. tuberculosis* infection, and thus *M. tuberculosis* has evolved numerous mechanisms for avoiding trafficking to lysosomes. Indeed, several screens have identified

mutants of *M. tuberculosis* that exhibit increased trafficking to lysosomes.[39,40] We have shown that WT *M. tuberculosis* exhibits increased trafficking to lysosomes in gefitinib-treated cells and that the increased number of lysosomes induced by gefitinib are functional. To establish that gefitinib-induced lysosomes are not only functional but bactericidal against *M. tuberculosis*, we tested whether *M. tuberculosis* mutants with increased trafficking to lysosomes (Tn:Rv2693c and Tn:MmpL9) are more susceptible to gefitinib-induced killing by macrophages. We infected macrophages with either WT or lysosomal mutant bacteria and treated the macrophages with gefitinib (Figure 5C). As previously published, we found that the lysosomal mutants exhibited increased trafficking to lysosomes in untreated macrophages (Figure 5D). The addition of gefitinib further increased the fraction of both WT and lysosomal mutants co-localization with lysosomes. We assessed the growth of WT compared to the lysosomal mutants in cells treated with gefitinib by CFU. Importantly, the lysosomal mutants exhibited enhanced susceptibility to gefitinib-mediated killing in macrophages compared with WT (Figure 5E), further supporting the hypothesis that gefitinib-induced lysosomes are functional and contribute to the cell intrinsic activity of this inhibitor.

The goal of HDT is to augment the current *M. tuberculosis* chemotherapies to shorten treatment times and reduce the development of drug resistance. We have demonstrated that gefitinib can regulate both cell-intrinsic properties and cell-extrinsic properties of macrophages that can contribute to the control of *M. tuberculosis* (Figure S3). Gefitinib treatment of macrophages increases lysosomal biogenesis, and there is an increase in trafficking of *M. tuberculosis* to lysosomes, which results in increased bacterial killing. In addition, gefitinib-treated macrophages could orchestrate a wider effect on the immune response to *M. tuberculosis* infection in vivo. For example, gefitinib treatment increases autophagic flux in macrophages, which may not be directly bactericidal in macrophages, but could increase antigen presentation and activation of the innate immune response. In addition, gefitinib treatment inhibits STAT3 activation and decreases the levels of IL-6 secreted from macrophages, which could promote Th1 T cell development in vivo, a hypothesis that will require future testing in vivo. These observations will motivate a more detailed examination of gefitinib's mechanism of action in vivo in both acute and chronic infection. Interestingly, the JAK/STAT inhibitor tofacitinib was recently shown to shorten treatment times when used as an adjunct to standard therapy in mice.[41,42] Tofacitinib less specifically inhibits JAK/STAT signaling and is therefore anti-inflammatory. When used as a sole agent, tofacitinib results in enhanced bacterial replication in *M. tuberculosis* infected mice, thereby making bacteria more susceptible to conventional antibiotics. Gefitinib, on the other hand, activates cell intrinsic control, restricts *M. tuberculosis* replication when used as a sole agent in vivo, and has the potential to augment Th1 responses. Importantly, as for any HDT, determining the efficacy of gefitinib in conjunction with current frontline antibiotics is a critical next step in evaluating the potential of gefitinib as a novel therapeutic. In conclusion, we have shown that gefitinib is a viable candidate as a host-directed therapy and provides an additional tool to study the mechanism of host-mediated control of *M. tuberculosis* infection.

METHODS

Ethics Statement

All procedures involving the use of mice were approved by the University of California—Berkeley, Institutional Animal Care and Use Committee (Protocol R353-1113B). All protocols conform to federal regulations, the National Research Council's Guide for the Care and Use of Laboratory Animals, and the Public Health Service's Policy on Humane Care and Use of Laboratory Animals.

Reagents

Gefitinib (S1025) was obtained from Selleck Chemicals and was used at 10 μM. Mouse rIFN-γ (485 MI/CF) was obtained from R&D Systems (Minneapolis, MN, USA) and was used at 6.25 ng/mL. Chloroquine (*C6628*) was obtained from Sigma-Aldrich (St. Louis, MO, USA).

Mice and Cell Culture

Wild-type (WT) mice were C57BL/6 and were obtained from The Jackson Laboratory (Bar Harbor, ME, USA). All knockout mice were backcrossed to C57BL/6. B6.129S1-Stat3tm1Xyfu/J mice were obtained from The Jackson Laboratory and were crossed with B6.129P2-Lyz2tm1(cre)Ifo/J to generate mice that had STAT3 deletion targeted to the myeloid lineage. BMDM were obtained by flushing cells from the femurs and tibias of mice and culturing in DMEM with 10% FBS and 10% supernatant from 3T3-M-CSF cells (BMDM media) for 6 days with feeding on day 3. After differentiation, BMDM continued to be cultured in BMDM media containing M-CSF.

Bacterial Culture

The *M. tuberculosis* strains Erdman and H37Rv were used in experiments as indicated. *M. tuberculosis* was grown in Middlebrook 7H9 liquid medium supplemented with 10% albumin–dextrose–saline, 0.4% glycerol, and 0.05% Tween 80 or on solid 7H10 agar plates supplemented with 10% Middlebrook OADC (BD Biosciences) and 0.4% glycerol. The TB-lux strain is a reporter strain that constitutively expresses the bacterial luciferase operon *lux*CDABE and was a gift from the Cox laboratory, University of California—Berkeley. The TB-lux, TB-GFP, or TB-635T strains used for measuring bacterial growth or fluorescent microscopy were derived from an Erdman strain unless noted otherwise and were cultured as described above. The transposon mutants Tn:Mmpl9 and Tn:Rv2693c were obtained from an arrayed library generated at the Broad Institute from *M. tuberculosis* strain H37Rv. Fluorescent strains of H37Rv and the transposon mutants were generated by transforming each strain with a plasmid containing eGFP under a MOP promoter as described previously.[43]

In Vitro Infections

BMDM were plated into 96- or 24-well plates with 5×10^4 and 2.5×10^5 macrophages/well, respectively, and were allowed to adhere and rest for 24 h. BMDM were infected in DMEM supplemented with 5% horse serum and 5% FBS at a multiplicity of infection of 1, unless

otherwise noted. After a 4 h phagocytosis period, infected BMDM were washed with PBS before replacing with BMDM medium with or without gefitinib treatment as indicated. For experiments with chloroquine and gefitinib, these reagents were added to the BMDM medium after the 4 h phagocytosis. For IFN-γ-activated cells, cells were treated with IFN-γ 18 h prior to infection, and IFN-γ was also added post-infection at the same concentration. To measure intracellular growth of *M. tuberculosis* by luminescence, cells were infected with TB-lux (Erdman), and luminescence was measured at 32 °C immediately following the 4 h phagocytosis, PBS wash, and medium replacement. Luminescence was then read again at the noted time points. All growth was normalized to day 0 luminescence readings for each infected well and is presented as fold change in luminescence compared with day 0. For enumeration of CFU, *M. tuberculosis* Erdman strain was used unless otherwise noted. Infected BMDM were washed with PBS and lysed in water with 0.1% Triton X-100 for 10 min, and serial dilutions were prepared in PBS with 0.05% Tween 80 and were plated onto 7H10 plates. Colonies were counted after 21 days.

Griess Assays

The Griess reaction was used to detect nitrite in the supernatants of BMDM as a proxy for NO production. Briefly, a solution of 0.2% naphthylethylenediamine dihydrochloride was mixed 1:1 with a 2% sulfanilamide, 4% phosphoric acid solution. A total of 50 μL of supernatant from cultured cells was added to 50 μL of Griess reagent, and absorbance was measured at 546 nm. Concentrations were determined by comparison to a standard curve of nitrite in BMDM medium.

Western Blots

Infected BMDM were washed with PBS, lysed in RIPA buffer (10 mM sodium phosphate, pH 7.2, 150 mM NaCl, 0.1% SDS, 1% sodium deoxycholate, 1% Triton X-100, 200 μM sodium vanadate, 100× protease/phosphatase inhibitor cocktail (5872, Cell Signaling Technology), 2 mM EDTA, 1 mM DTT) on ice and heat sterilized for 30 min at 100 °C. Total protein lysates were analyzed by SDS-PAGE using precast Tris-HCl criterion gels (Bio-Rad, Hercules, CA, USA). The following primary Abs were used: rabbit Ab against LC3 (2775S; Cell Signaling Technology, Danvers, MA, USA), STAT3 (D3Z2G; Cell Signaling Technology), pSTAT3-Tyr705 (M9C6, Cell Signaling Technology). HRP-conjugated secondary Abs were used: anti-rabbit-HRP (sc-2030; Santa Cruz Biotechnology, Santa Cruz, CA, USA), anti-mouse-HRP (7076, Cell Signaling Technology). Western Lightning Plus-ECL chemiluminescence substrate (Perkin- Elmer, Waltham, MA, USA) was used, and blots were developed using a ChemiDoc MP System (Bio-Rad). Blots were stripped using 0.2 M NaOH and then washed in ddH_2O and TBST before blocking and reprobing for actin as a loading control, using a HRP-conjugated rabbit Ab against β-actin (13E5; Cell Signaling Technology).

Immunofluorescence

BMDM were plated on coverslips in 24-well plates and infected as previously described. At the indicated time points, coverslips were washed in room temperature 1× PBS and fixed with 4% PFA for 20 min at room temperature. PFA was washed and coverslips were stored in PBS until stained. Cells were permeablized and stained in 1% BSA and 0.1% saponin in

1× PBS. For LAMP1 staining (rat anti-LAMP1 conjugated to AF647, 121609; Biolegend, San Diego, CA, USA) cells were incubated with antibody at 1:1000 dilution overnight at 4 °C. For LC3-GFP staining, cells were incubated with a mouse-anti-GFP antibody (11814460001, Sigma-Aldrich, St. Louis, MO, USA) for 90 min at room temperature. Cells were washed and stained with an anti-mouse-AF488 (#4408, Cell Signaling) for 1 h at room temperature. Lysosomal staining was done live at the indicated time point. At the indicated time points, medium was replaced with full medium, including drug or cytokine treatments, with 50 nM Lysotracker red DND-99 (#L7528, ThermoFisher Scientific, Waltham, MA, USA) for 1 h at 37 °C. Cells were washed with room temperature 1× PBS before fixing as previously described. Cells were imaged immediately after fixing. For labeling with DQ-BSA (D12050, ThermoFisher Scientific), cells were pulsed with 10 μg/mL DQ-BSA and incubated at 37 °C,; after 1 h, cells were chased with medium (± drug) without DQ-BSA for 1 h before washing and fixing. Cells were imaged immediately after fixing. Coverslips were imaged on a confocal microscope (Zeiss LSM 710).

RNA-seq

For RNA-seq, three independent experiments were performed. BMDM were seeded in 24-well dishes at 3×10^5 cells per well and infected, as described. At 4 and 24 h post-infection, cells were washed with room temperature PBS and lysed in 500 μL of TRIzol (Invitrogen Life Technologies, Carlsbad, CA, USA). Total RNA was extracted using chloroform (100 μL), and the aqueous layer was further purified using RNeasy spin columns (Qiagen, Limburg, Germany). For each sample in each experiment, two duplicate wells were pooled. RNA-seq was performed at the Genome Center and Bioinformatics Core Facility at the University of California—Davis (Davis, CA, USA). SR50 reads were run on an Illumina HiSeq3000, with ~30 million reads per sample. Data analysis was performed by the University of California—Davis bioinformatics group using FastQC for read quality assessment, Sythe and Sickle for Illumina adapter and quality trimming, and Tophat2 for read alignment. Raw counts were derived from alignments using a STSeq-count python script.[44] Tests of differential expression were conducted using a multifactorial model in edgeR/limma (voom).

Phosphoproteomics

BMDM were plated at 3×10^7 cells in T-flasks and infected as previously described. At 4 and 8 h post-infection, cells were fixed in ice-cold MeOH, wiped out of the BSL3. Cells were washed with ice-cold PBS and lysed in lysis buffer (made fresh before each replicate, 8 M urea, 150 mM NaCl, 100 mM ammonium bicarbonate, pH 8; added per 10 mL of buffer: 1 tablet of Roche mini-complete protease inhibitor EDTA free (catalog no. 04693159001) and 1 tablet of Roche Phosphostop mini tablet (catalog no. 04906845001)). Lysate was centrifuged at 4 °C to remove any precipitate and put at −80 °C until analysis. A Bradford assay was performed to measure protein concentration, and 10 mg of each sample was used for subsequent processing. Lysates were sonicated three times at 30% power and then reduced with 4 mM tris(2-carboxyethyl)phosphine for 30 min at room temperature and alkylated with 2 mM iodoacetamide for 30 min at room temperature in the dark. Samples were diluted 4-fold to reduce urea concentration to below 2 M, and trypsin was added at a 1:100 enyzme/substrate ratio for overnight digestion at 37 °C. Samples were desalted using

SepPak tC18 solid-phase extraction cartridges (Waters). Cartridges were washed with 1 mL of 80% ACN and then with 3 mL of 0.1% TFA; samples were loaded and then washed with 3 mL of 0.1% TFA and eluted with 1 mL of 40% ACN, 0.1% TFA. The elution was lyophilized completely for 2 days to remove any TFA remaining in the elution. Phosphotyrosine-containing peptides were enriched by immunopurification using a PTMScan phosphotyrosine purification kit (Cell Signaling).

Mass Spectrometry Analysis

Phosphotyrosine-enriched peptides were analyzed in technical duplicate on a Thermo-Fisher Orbitrap Fusion mass spectrometry system equipped with an Easy nLC 1200 ultrahigh-pressure liquid chromatography system interfaced via a Nanospray Flex nanoelectrospray source. Samples were injected on a C18 reverse phase column (25 cm × 75 μm packed with ReprosilPur C18 AQ 1.9 um particles). Peptides were separated by an organic gradient from 5 to 30% ACN in 0.1% formic acid over 112 min at a flow rate of 300 nL/min. The MS continuously acquired spectra in a data-dependent manner throughout the gradient, acquiring a full scan in the Orbitrap (at 120,000 resolution with an AGC target of 200,000 and a maximum injection time of 100 ms) followed by as many MS/MS scans as could be acquired on the most abundant ions in 3 s in the dual linear ion trap (rapid scan type with an intensity threshold of 5000, HCD collision energy of 29%, AGC target of 10,000, maximum injection time of 35 ms, and isolation width of 1.6 m/z). Singly and unassigned charge states were rejected. Dynamic exclusion was enabled with a repeat count of 1, an exclusion duration of 20 s, and an exclusion mass width of ±10 ppm. Raw mass spectrometry data were assigned to human protein sequences and MS1 intensities extracted with the MaxQuant software package (version 1.5.5.1).[45] Data were searched against the SwissProt human protein database (downloaded on January 11, 2016). Variable modifications were allowed for N-terminal protein acetylation, methionine oxidation, and tyrosine phosphorylation. A static modification was indicated for carbamidomethyl cysteine. All other settings were left using MaxQuant default settings.

The MaxQuant-analyzed data were subsequently analyzed using an in-house computational pipeline for statistical analysis of relative quantification with fixed and/or mixed effect models, implemented in the MSstats Bioconductor package (version 3.3.10).[46] Contaminants, decoy hits, and peptides not containing acetyllysine residues were removed, and all samples were normalized across fractions by median-centering the log2-transformed MS1 intensity distributions. Then, the MSstats group comparison function was run with the following options: no interaction terms for missing values, no interference, unequal intensity feature variance, restricted technical and biological scope of replication. Statistically significantly changing sites were selected by applying a log2-fold-change (>1.0) and an adjusted p value (<0.05) corrected for multiple testing threshold. Phosphotyrosine log2-fold-change profiles were uploaded to the PhosFate Profiler tool (Phosfate.com[26]) to identify published phosphoproteomics data sets with significant correlations. Correlations with p values <0.05 are illustrated in Figure 2C. Hierarchical clustering of phosphotyr-osine profiles was performed using Cluster 3.0,[47] and clusters were visualized using Java TreeView.[48] Enrichment analysis of significantly overrepresented gene ontology terms in

clusters was performed using Metascape using the proteins in a cluster as the foreground and using all proteins detected as the background.[49]

Bacterial Co-localization Measurements

BMDM were plated in black 96-well sensoplates (no. 655892, Greiner bio, Austria). Cells were infected as previously described with eGFP expressing H37Rv, Tn:MmpL9, or Tn:Rv2693c. At 24 h, cells were stained live with Lysotracker red and fixed. Cells were washed with PBS and imaged on Automated Epifluorescence Microscopy ImageXpress Micro (Molecular Devices, Sunny-vale, CA, USA) using a 20× PA objective. Images were analyzed by Cell Profiler.

Image Analysis

Images were analyzed using Cell Profiler open-source software.[50] The imaging analysis pipeline is openly available (http://cellprofiler.org/published_pipelines.shtml) and included quantification of pixel intensity, co-localization, and object counting.

Supplementary Material

Refer to Web version on PubMed Central for supplementary material.

Acknowledgments

LC3-GFP BMDM were a gift from Daniel Portnoy's laboratory at University of California—Berkeley. Femurs from Atg7 flox/flox and Atg7 flox/flox LysMcre +/+ mice were a gift from Christina Stallings at Washington University Saint Louis. This work was performed in part at the CRL Molecular Imaging Center, supported by the Gordon and Betty Moore Foundation. We thank Dr. Mary West and Dr. Pingping He of the QB3 High Throughput Screening Facility (HTSF) at University of California—Berkeley. This work was performed in part in the HTSF, which provided the Molecular Devices Image Xpress Micro. We give special thanks to Jonathan Braverman and Ayush Kumar for technical assistance. This work was supported by NIH Grant 1R21AI110863-01 to S.A.S. Funding support for K.M.S. was provided by T32 AI 100829-4.

References

1. Floyd, K. Global Tuberculosis Report. World Health Organization; 2016.
2. Dartois V. The Path of Anti-Tuberculosis Drugs: From Blood to Lesions to Mycobacterial Cells. Nature Publishing Group. 2014; 12(3):159–167. DOI: 10.1038/nrmicro3200
3. World Health Organization. Guidelines for the Programmatic Management of Drug-Resistant Tuberculosis. 2011
4. Hawn TR, Matheson AI, Maley SN, Vandal O. Host-directed therapeutics for tuberculosis: can we harness the host? Microbiol Mol Biol Rev: MMBR. 2013; 77(4):608–627. [PubMed: 24296574]
5. Hawn TR, Shah JA, Kalman D. New tricks for old dogs: countering antibiotic resistance in tuberculosis with host-directed therapeutics. Immunol Rev. 2015; 264(1):344–362. [PubMed: 25703571]
6. Stanley SA, Barczak AK, Silvis MR, Luo SS, Sogi K, Vokes M, Bray M-A, Carpenter AE, Moore CB, Siddiqi N, et al. Identification of host-targeted small molecules that restrict intracellular *Mycobacterium tuberculosis* growth. PLoS Pathog. 2014; 10(2):e1003946. [PubMed: 24586159]
7. Wieduwilt MJ, Moasser MM. The epidermal growth factor receptor family: biology driving targeted therapeutics. Cell Mol Life Sci. 2008; 65(10):1566–1584. [PubMed: 18259690]
8. Bazley LA, Gullick WJ. Epidermal growth factor receptor family. Endocr-Relat Cancer. 2005; 12(Suppl 1):S17–S27. [PubMed: 16113093]

9. Ellis PM, Coakley N, Feld R, Kuruvilla S, Ung YC. Use of the epidermal growth factor receptor inhibitors gefitinib, erlotinib, afatinib, dacomitinib, and icotinib in the treatment of non-small-cell lung cancer: a systematic review. Curr Oncol (Toronto, Ont). 2015; 22(3):e183–e215.
10. Eierhoff T, Hrincius ER, Rescher U, Ludwig S, Ehrhardt C. The epidermal growth factor receptor (EGFR) promotes uptake of influenza A viruses (IAV) into host cells. PLoS Pathog. 2010; 6(9):e1001099. [PubMed: 20844577]
11. Liu K, Gualano RC, Hibbs ML, Anderson GP, Bozinovski S. Epidermal growth factor receptor signaling to Erk1/2 and STATs control the intensity of the epithelial inflammatory responses to rhinovirus infection. J Biol Chem. 2008; 283(15):9977–9985. [PubMed: 18276593]
12. Yan F, Cao H, Chaturvedi R, Krishna U, Hobbs SS, Dempsey PJ, Peek RM, Cover TL, Washington MK, Wilson KT, et al. Epidermal growth factor receptor activation protects gastric epithelial cells from *Helicobacter pylori*-induced apoptosis. Gastroenterology. 2009; 136(4):1297–1307. [PubMed: 19250983]
13. Kumar D, Nath L, Kamal MA, Varshney A, Jain A, Singh S, Rao KVS. Cell. 2010; 140(5):731–743. [PubMed: 20211141]
14. Jayaswal S, Kamal MA, Dua R, Gupta S, Majumdar T, Das G, Kumar D, Rao KVS. Identification of host-dependent survival factors for intracellular *Mycobacterium tuberculosis* through an siRNA screen. PLoS Pathog. 2010; 6(4):e1000839. [PubMed: 20419122]
15. Tobin DM, Vary JC, Ray JP, Walsh GS, Dunstan SJ, Bang ND, Hagge DA, Khadge S, King M-C, Hawn TR, et al. Cell. 2010; 140(5):717–730. [PubMed: 20211140]
16. Tapinos N, Ohnishi M, Rambukkana A. ErbB2 receptor tyrosine kinase signaling mediates early demyelination induced by leprosy bacilli. Nat Med. 2006; 12(8):961–966. [PubMed: 16892039]
17. Muniz-Feliciano L, Van Grol J, Portillo J-AC, Liew L, Liu B, Carlin CR, Carruthers VB, Matthews S, Subauste CS. *Toxoplasma gondii*-induced activation of EGFR prevents autophagy protein-mediated killing of the parasite. PLoS Pathog. 2013; 9(12):e1003809. [PubMed: 24367261]
18. Lanaya H, Natarajan A, Komposch K, Li L, Amberg N, Chen L, Wculek SK, Hammer M, Zenz R, Peck-Radosavljevic M, et al. EGFR has a tumour-promoting role in liver macrophages during hepatocellular carcinoma formation. Nat Cell Biol. 2014; 16(10):972–981. [PubMed: 25173978]
19. Lu N, Wang L, Cao H, Liu L, Van Kaer L, Washington MK, Rosen MJ, Dube PE, Wilson KT, Ren X, et al. J Immunol. 2014; 192(3):1013–1023. [PubMed: 24391216]
20. Rottenberg ME, Carow B. SOCS3 and STAT3, major controllers of the outcome of infection with *Mycobacterium tuberculosis*. Semin Immunol. 2014; 26(6):518–532. [PubMed: 25458989]
21. Gutierrez MG, Master SS, Singh SB, Taylor GA, Colombo MI, Deretic V. Cell. 2004; 119(6):753–766. [PubMed: 15607973]
22. MacMicking JD, North RJ, LaCourse R, Mudgett JS, Shah SK, Nathan CF. Identification of nitric oxide synthase as a protective locus against tuberculosis. Proc Natl Acad Sci U S A. 1997; 94(10): 5243–5248. [PubMed: 9144222]
23. Braverman J, Sogi KM, Benjamin D, Nomura DK, Stanley SA. J Immunol. 2016; 197(4):1287–1297. [PubMed: 27430718]
24. Glick D, Barth S, Macleod KF. Autophagy: cellular and molecular mechanisms. J Pathol. 2010; 221(1):3–12. [PubMed: 20225336]
25. Tanida I, Minematsu-Ikeguchi N, Ueno T, Kominami E. Lysosomal turnover, but not a cellular level, of endogenous LC3 is a marker for autophagy. Autophagy. 2005; 1(2):84–91. [PubMed: 16874052]
26. Ochoa D, Jonikas M, Lawrence RT, Debs El B, Selkrig J, Typas A, Villen J, Santos SD, Beltrao P. An atlas of human kinase regulation. Mol Syst Biol. 2016; 12(12):888. [PubMed: 27909043]
27. Schmutz C, Ahrné E, Kasper CA, Tschon T, Sorg I, Dreier RF, Schmidt A, Arrieumerlou C. Systems-level overview of host protein phosphorylation during *Shigella flexneri* infection revealed by phosphoproteomics. Mol Cell Proteomics. 2013; 12(10):2952–2968. [PubMed: 23828894]
28. Rogers LD, Brown NF, Fang Y, Pelech S, Foster LJ. Phosphoproteomic analysis of *Salmonella*-infected cells identifies key kinase regulators and SopB-dependent host phosphor-ylation events. Sci Signaling. 2011; 4(191):rs9–rs9.

29. Pan C, Olsen JV, Daub H, Mann M. Global effects of kinase inhibitors on signaling networks revealed by quantitative phosphoproteomics. Mol Cell Proteomics. 2009; 8(12):2796–2808. [PubMed: 19651622]
30. Queval CJ, Song OR, Deboosére N, Delorme V, Debrie AS, Iantomasi R, Veyron-Churlet R, Jouny S, Redhage K, Deloison G, et al. STAT3 represses nitric oxide synthesis in human macrophages upon *Mycobacterium tuberculosis* infection. Sci Rep. 2016; 6:29297. [PubMed: 27384401]
31. Takeda K, Clausen BE, Kaisho T, Tsujimura T, Terada N, Förster I, Akira S. Enhanced Th1 activity and development of chronic enterocolitis in mice devoid of Stat3 in macrophages and neutrophils. Immunity. 1999; 10(1):39–49. [PubMed: 10023769]
32. Melillo JA, Song L, Bhagat G, Blazquez AB, Plumlee CR, Lee C, Berin C, Reizis B, Schindler C. Dendritic cell (DC)-specific targeting reveals Stat3 as a negative regulator of DC function. J Immunol. 2010; 184(5):2638–2645. [PubMed: 20124100]
33. Carow B, Reuschl A-K, Gavier-Widén D, Jenkins BJ, Ernst M, Yoshimura A, Chambers BJ, Rottenberg ME. Critical and independent role for SOCS3 in either myeloid or T cells in resistance to *Mycobacterium tuberculosis*. PLoS Pathog. 2013; 9(7):e1003442. [PubMed: 23853585]
34. Green AM, DiFazio R, Flynn JL. IFN- from CD4 T cells is essential for host survival and enhances CD8 T cell function during *Mycobacterium tuberculosis* infection. J Immunol. 2013; 190(1):270–277. [PubMed: 23233724]
35. Yu H, Pardoll D, Jove R. STATs in cancer inflammation and immunity: a leading role for STAT3. Nat Rev Cancer. 2009; 9(11):798–809. [PubMed: 19851315]
36. Scaltriti M, Baselga J. The epidermal growth factor receptor pathway: a model for targeted therapy. Clin Cancer Res. 2006; 12(18):5268–5272. [PubMed: 17000658]
37. Appelqvist H, Wäster P, Kågedal K, Öllinger K. The lysosome: from waste bag to potential therapeutic target. J Mol Cell Biol. 2013; 5(4):214–226. [PubMed: 23918283]
38. Nadanaciva S, Lu S, Gebhard DF, Jessen BA, Pennie WD, Will Y. A high content screening assay for identifying lysosomotropic compounds. Toxicol In Vitro. 2011; 25(3):715–723. [PubMed: 21184822]
39. MacGurn JA, Cox JS. A genetic screen for *Mycobacterium tuberculosis* mutants defective for phagosome maturation arrest identifies components of the ESX-1 secretion system. Infect Immunity. 2007; 75(6):2668–2678. [PubMed: 17353284]
40. Pethe K, Swenson DL, Alonso S, Anderson J, Wang C, Russell DG. Isolation of *Mycobacterium tuberculosis* mutants defective in the arrest of phagosome maturation. Proc Natl Acad Sci U S A. 2004; 101(37):13642–13647. [PubMed: 15340136]
41. Maiga M, Lun S, Guo H, Winglee K, Ammerman NC, Bishai WR. Risk of tuberculosis reactivation with tofacitinib (CP-690550). J Infect Dis. 2012; 205(11):1705–1708. [PubMed: 22474037]
42. Maiga M, Ahidjo BA, Maiga MC, Cheung L, Pelly S, Lun S, Bougoudogo F, Bishai WR. Efficacy of adjunctive tofacitinib therapy in mouse models of tuberculosis. EBioMedicine. 2015; 2(8):868–873. [PubMed: 26425693]
43. Stanley SA, Grant SS, Kawate T, Iwase N, Shimizu M, Wivagg C, Silvis M, Kazyanskaya E, Aquadro J, Golas A, et al. Identification of novel inhibitors of *M. tuberculosis* growth using whole cell based high-throughput screening. ACS Chem Biol. 2012; 7(8):1377–1384. [PubMed: 22577943]
44. Anders S, Pyl PT, Huber W. HTSeq—a Python framework to work with high-throughput sequencing data. Bio-informatics. 2015; 31(2):166–169.
45. Cox J, Mann M. MaxQuant enables high peptide identification rates, individualized p.p.b.-range mass accuracies and proteome-wide protein quantification. Nat Biotechnol. 2008; 26(12):1367–1372. [PubMed: 19029910]
46. Choi M, Chang C-Y, Clough T, Broudy D, Killeen T, MacLean B, Vitek O. MSstats: an R package for statistical analysis of quantitative mass spectrometry-based proteomic experiments. Bioinformatics. 2014; 30(17):2524–2526. [PubMed: 24794931]
47. de Hoon MJL, Imoto S, Nolan J, Miyano S. Open source clustering software. Bioinformatics. 2004; 20(9):1453–1454. [PubMed: 14871861]

48. Saldanha AJ. Java Treeview—extensible visualization of microarray data. Bioinformatics. 2004; 20(17):3246–3248. [PubMed: 15180930]

49. Tripathi S, Pohl MO, Zhou Y, Rodriguez-Frandsen A, Wang G, Stein DA, Moulton HM, DeJesus P, Che J, Mulder LCF, et al. Meta- and orthogonal integration of influenza "OMICs" data defines a role for UBR4 in virus budding. Cell Host Microbe. 2015; 18(6):723–735. [PubMed: 26651948]

50. Carpenter AE, Jones TR, Lamprecht MR, Clarke C, Kang IH, Friman O, Guertin DA, Chang JH, Lindquist RA, Moffat J, et al. CellProfiler: image analysis software for identifying and quantifying cell phenotypes. Genome Biol. 2006; 7(10):R100. [PubMed: 17076895]

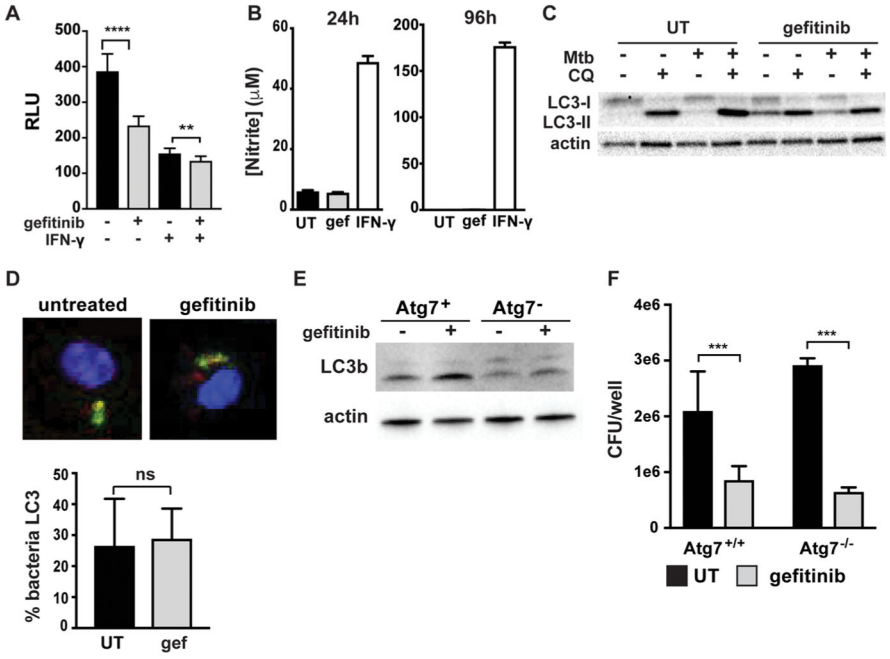

Figure 1.

(A) Resting and IFN-γ-activated WT BMDM were infected with the TB-lux strain of *M. tuberculosis*. Bacterial growth was assessed by reading relative light units at 96 hpi. (B) Griess assay for NO production at 24 and 96 h post-infection. (C) Western blot of LC3b from cell lysates taken 4 h after drug treatment with actin as the loading control. (D) Immunofluorescence of LC3-GFP co-localized with *M. tuberculosis* expressing 635Turbo fluorescent protein. (E) Western blot of LC3 from protein lysates from Atg7+ and Atg7− cells after 4 h of gefitinib treatment (representative experiment of two replicates). (F) Atg7+ and Atg7− BMDM were infected with *M. tuberculosis* at a multiplicity of infection of 1, and bacterial growth was measured at 4 days post-infection by CFU (representative of two replicates). For all experiments, error bars represent the SD of a minimum of triplicate wells, and a representative experiment of a minimum of three is shown unless noted otherwise. The *p* values were determined using an unpaired *t* test: (*)$p \leq 0.05$, (**) $p \leq 0.01$, (***) $p \leq 0.001$, and (****) $p \leq 0.0001$.

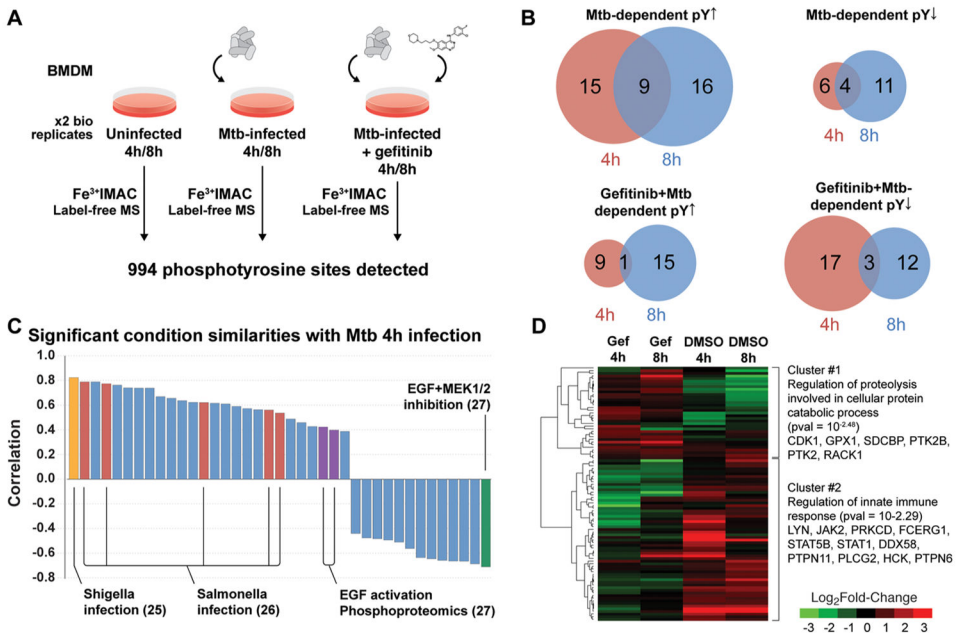

Figure 2.

(A) Summary of experimental design. (B) Venn diagrams of identified phosphotyrosine sites at each time point for *M. tuberculosis* infected macrophages. *M. tuberculosis*-dependent peptides are from a comparison of infected to mock infected, and gefitinib-dependent peptides are from a comparison of *M. tuberculosis* infected DMSO-treated to *M. tuberculosis* infected gefitinib-treated peptides. (C) Comparison of the *M. tuberculosis* 4 h infected (untreated) phosphoproteomics profile to a curated database of published phosphoproteomics studies using Phosfate.com. Each bar represents a phosphoproteomics data set in PhosFate with significant correlation with our data set with *Shigella* infection conditions in light orange, *Salmonella* infection conditions in dark orange, EGF activation in purple, and EGF inhibition in green. Only significant ($p < 0.05$) correlations are plotted. (D) Hierarchical clustering of L2FC values for *M. tuberculosis* 4 h versus mock, *M. tuberculosis* 8 h versus mock, Gef 4 h versus *M. tuberculosis* 4 h, and Gef 8 h versus *M. tuberculosis* 8 h. Sites are included in clustering analysis if they are significant (|L2FC| > 1 and pval <0.05) in at least one comparison. Sites must be detected in all conditions to be included. Cluster divides into two well-separated clusters and some smaller clusters. GO term enrichments of the two large clusters are indicated to the right of the heatmap.

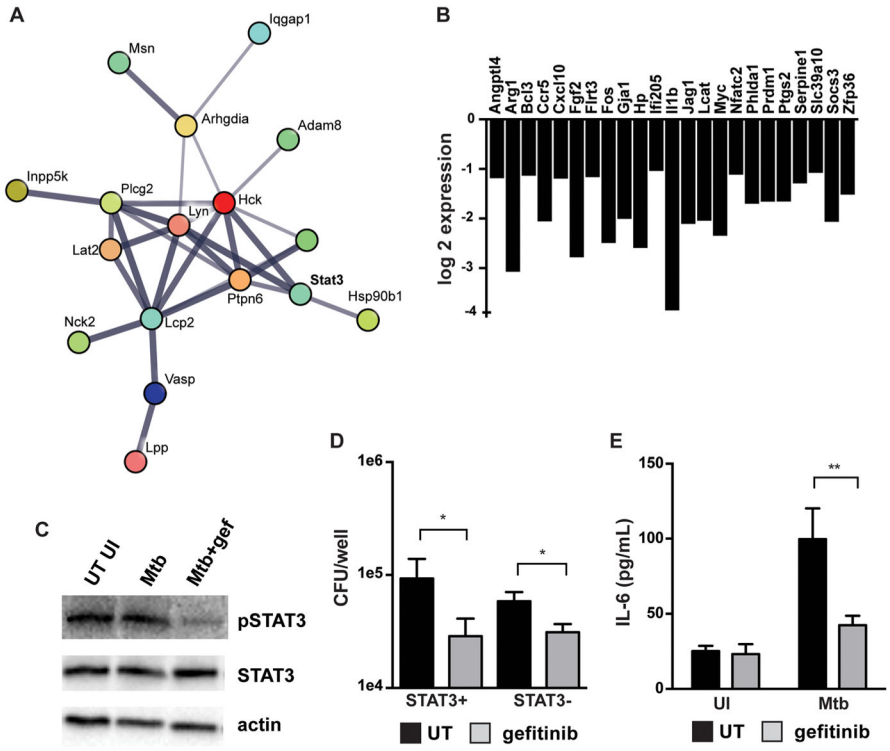

Figure 3.

(A) Protein interaction map depicting the proteins with the greatest change in phosphorylation state after 4 h of gefitinib treatment produced through the STRING web resource. (B) log2 expression of STAT3 target genes from RNA-seq analysis at 4 h post-infection. (C) Western blot of phospho-STAT3 Y705 (pSTAT3) and total STAT3 protein from cell lysates taken 24 h post-infection. Actin is shown as a loading control. (D) $STAT3^{+}$ and $STAT3^{-}$ BMDM were infected with *M. tuberculosis* at a multiplicity of infection of 1, and bacterial growth was measured at 4 days post-infection by CFU (representative of three independent experiments). (E) ELISA for IL-6 in cell supernatants measured at 24 h post-infection. Representative of two independent experiments. For all experiments, error bars represent the SD of a minimum of triplicates. The p values were determined using an unpaired t test: (*) $p \leq 0.05$ and (**) $p \leq 0.01$.

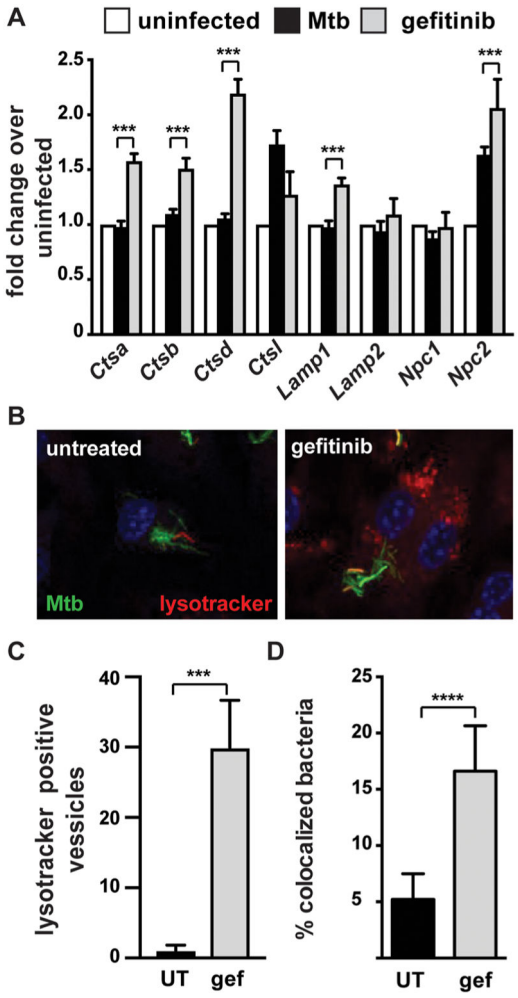

Figure 4.

(A) Total RNA reads of lysosomal genes represented as fold change over untreated uninfected cells at 24 h post-infection. The *p* values were determined using a two-way ANOVA Tukey's test: (***) $p \leq 0.001$. (B) Fluorescent imaging of BMDM infected with *M. tuberculosis* expressing eGFP at an MOI of 1 and stained with lysotracker and DAPI at 24 h post-infection. (C) Quantification of lysosomes per cell by Cell Profiler. (D) Bacterial co-localization quantification of (B) from 32 wells in a 96-well plate with 9 images per well. For (C) and (D): (***) $p \leq 0.001$ and (****) *p* value ≤0.0001 by Student's *t* test. For all experiments, error bars represent the SD of a minimum of triplicate wells, and a representative experiment of a minimum of three is shown unless noted otherwise.

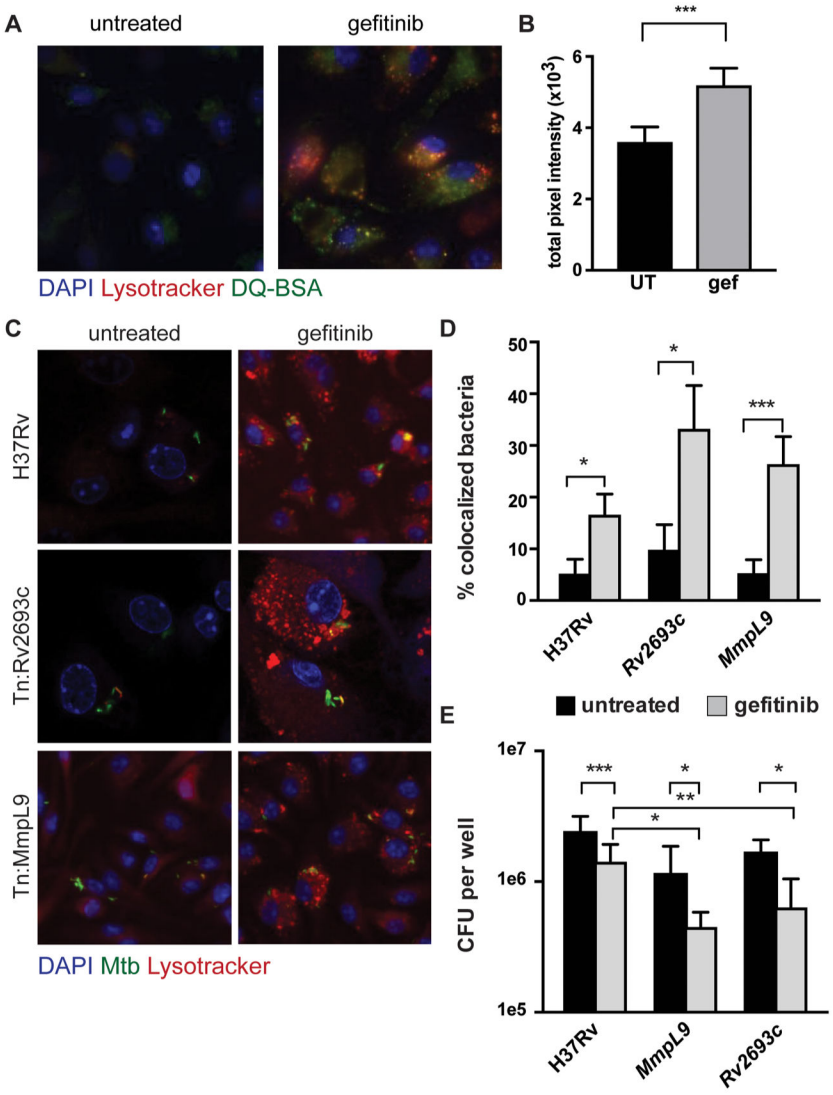

Figure 5.

(A) Fluorescent images of BMDM stained with DQ-BSA and lysotracker red DND-99 at 24 h post-infection with *M. tuberculosis* (not fluorescently labeled). (B) Quantification of (A) for total pixel intensity of DQ-BSA using Cell Profiler. (C) Fluorescent images of BMDM stained with lysotracker and infected with H37Rv or transposon mutants (Tn:Rv2693c and Tn:MmpL9) expressing eGFP (MOI = 1) at 24 h post-infection. (D) Quantification of bacterial co-localization of (C). (E) CFU from BMDM infected at a MOI of 1 with H37Rv, Tn:Rv2693c, or Tn:MmpL9 at 4 days post-infection. For all experiments, error bars represent the SD of a minimum of triplicate wells, and a representative experiment of a minimum of three is shown unless noted otherwise. The p values were determined using an unpaired t test: (*) $p \leq 0.05$ and (***) $p \leq 0.001$.